Micro-abrasion - corrosion of a Co-Cr/UHMWPE couple in Ringer's solution: an approach to construction of mechanism and synergism maps for application to bio-implants

M.M. Stack* , J. Jirka , M. T. Mathew, H. Jawan,

W. Huang, G. Park and C. Hodge

Department of Mechanical Engineering,

University of Strathclyde,

75 Montrose St.,

Glasgow,

G1 1XJ,

UK.

*Corresponding author

Telephone : 44-141-5483754, Fax:44 -141-5525105

E-mail: m.m.stack@mecheng.strath.ac.uk

1. Abstract

In studies of tribo-corrosion, the degradation of bio-materials has become of increasing research interest in recent years. This is because, in many cases, the interactions of the tribological and corrosion component in biological environments are not well understood. Moreover, the wide range of variables involved in the tribo-corrosion process, and the variety of materials used in such conditions, means that there are few systematic studies where materials and operating conditions are optimized.

In the total replacement of hip joints, the Co-Cr/UHMWPE couple has been used widely. However, the application of any replacement joint for biological conditions will depend on many factors including the activity of the patient and the overall load imposed on the artificial joint. This means evaluation of the tribo-corrosion behaviour over a multi parameter space is important in order to asssess the degradation possible for many patient/activity and body mass categories.

In this work, the performance of a Co-Cr/UHMWPE couple was evaluated in Ringer's solution in a tribological situation where micron size particles particles were entrained in the contact – micro-abrasion-corrosion. The effects of applied load and potential were invesigated in the study. Micro-abrasion-corrosion maps were constructed for the material indicaing the mechanism of degradation, the extent of wastage and of synergy/antagonism involved in the tribo-corrosion interaction.

2. Introduction

In the bio-materials field, a vast number of materials have been used in the construction of total replacement hip joints including ceramics, metals and plastics. Early research, however, indicated significant metal particle wear which arose during the product life cycle (1).

The first modern prosthetics based on a Co-Cr/ Polymer couple was developed by Charnley (1). Initial polymers included Teflon, Polyacetal and Polyesters. However due to high-rates of clinical failure such materials have been replaced in recent years by the use of UHMWPE. In the replacement of the femur materials, Co-Cr alloys are candidate alloys due to the formation of a chromium oxide layer on the surface which grows slowly and is adherent.

The combined effect of applied load to the surface i.e during motion and the effect of a very corrosive environment, such as the human body, can cause significant degradation of the joint surface. In particular, small debris of micron sized particles can form in the tribological contact and contribute to a more severe wear effect by micro-abrasion. It has also been shown that the presence of many of the corrosive by-products can lead to patient problems including necrosis, fibrosis and inflammation (2).

For hip joints, the maximum pressure generated during daily activities on the hip joint has been estimated at 12 MPa in acetabular cups (3). By considering a factor of safety of two, the maximum pressure used in this study was 25 MPa. (The load on the sample was calculated from Hertzian contact pressure, which was developed at the contact point between the femoral head and acetabular cups.) In some reported studies, expected pressure was approximated to a very high value of 375 MPa, to accelerate the expected wear events (4-5).

Recent work (6) has shown that proteins have a significant effect on the corrosion rate of Co-Cr-Mo implants. The presence of proteins in the abrasive test slurry can affect the cathodic kinetics. The protein enhanced interaction is interpreted in terms of its effect in the particle entrainment process.

Some recent work (7) in micro-abrasion-corrosion has concentrated on the construction of engineering maps to characterise the wear mechanisms, wastage regimes and the various tribo-corrosion interactions involved in micro-abrasion-corrosion have also been studied (8-9). There has been significant interest in micro-abrasion mechanisms (10) in recent years and regimes of micro-abrasion have been identified. The corrosion behaviour of Co-Cr and UHMWPE in simulated biological solutions has also been studied (11-14).

However, to date there have been few studies where the concepts of trbo-corrosion maps, micro-abrasion mechanisms, and a bio-material couple have been investigated simultaneously. The aim of this study is to address this issue. Here, the effect of

applied load and potential have been used to generate a range of tribo-corrosion maps for Co-Cr/UHMWPE in a laboratory simulated biological environment- Ringer's solution. The potential application of such maps to in-vivo environments is discussed in this paper.

3 Experimental details

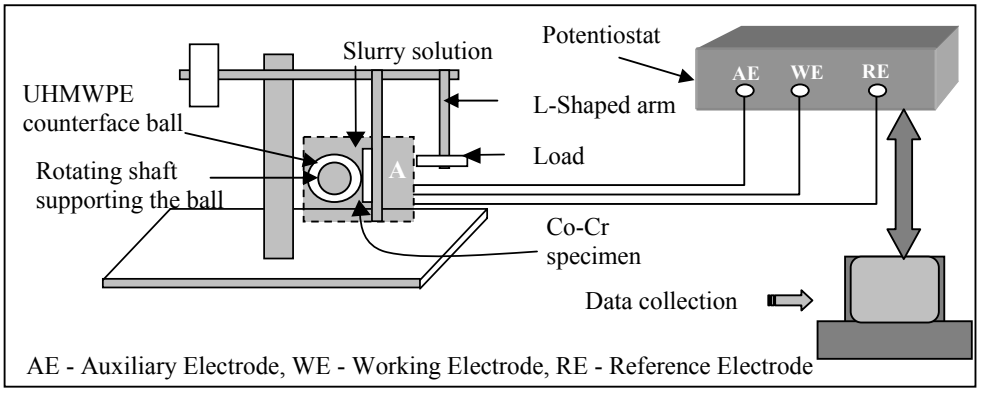

Figure 1. Schematic diagram of the micro-abrasion-corrosion apparatus

Micro-abrasion tests were performed with the TE-66, micro-abrasion tester, Figure. 1 (Plint and partners (Phoenix, UK)). The details of the experimental rig are as follows. A (25.4mm ball was located between two-coaxial shafts, each carried in a support bearing, with one of the shafts driven by a variable speed DC geared motor. A batch counter was provided to measure and control the number of shaft revolutions. A peristaltic pump head was connected to the other end of the shaft and this was used

for providing slurry feed to the contact. The test sample was clamped onto a platform, which was fitted to the pivoted L-shaped arm. This arm was rotated around its pivot until the sample came into contact with the ball. The load was applied by adding dead weights to a cantilever arm. It is important to note that this was not an attempt to directly simulate hip joint conditions but instead to demonstrate the application of the concept of the micro-abrasion-corrosion map to a bio-material couple, where the analogy may be made to wear in artificial hip joints. The slurry (concentration of 0.25 g cm^{-3}) was fed to a position just above the contact point and collected in a waste tray underneath. The relatively high concentration of SiC particles was used as to accelerate the test in order to simulate transitions between possible tribo-corrosion regimes. The specification of the apparatus is shown in Table 1.

Model	TE-66
Supplier	Phoenix tribology (Plint), UK.
Load range	0.05 to 5 N
Ball diameter	25 mm
Ball speed range	30 - 150 rpm
Pump feed rate	To 1 ml s^{-1} (Based on 0.5mm bore)

Table 1. Specification of micro-abrasion apparatus

The arm, which holds the sample, could be moved horizontally in order that several tests on a single sample specimen could be carried out. (It is recognized that with this arrangement, the actual load may deviate, particularly if the specimen looses contact with the ball at higher rotational speeds, where some experimental stability may set

in). The sample was then removed from the apparatus and the diameter of the resulting abrasion scars was measured with profile projector and optical microscope.

The material of the ball used was UHMWPE and was selected as stated above because it provided an inert surface against which corrosion of the counterface could be measured during the micro-abrasion test. The (Co-Cr) surfaces were ground and polished by conventional metallographic methods before testing. Following the test, the worn samples were examined by optical, scanning electron and atomic force microscopy in addition to profilometric methods. Repeat tests were carried out at various loads; the error in the experimental data was estimated to be $\pm$ 20 %.

The wear volume was calculated using the standard technique (13) for measuring the wear scar of spherical geometry(11) i.e. the geometry of the wear scar is assumed to reproduce the spherical geometry of the ball, and the wear volume (V) may then be calculated by measuring the crater diameter (b)

$$V \approx \pi b^4 \ (64\ R)^{-1} \quad \text{For } b << R \qquad (1)$$

The corrosive slurry of (Ringer's solution, Table 2) and SiC 4µm particles, was stored in a container that could be agitated by means of a laboratory magnetic stirrer and was delivered to the specimen by an integral peristaltic pump. Hence, the surface of the wear scar was immersed during the test. The pH of the solution was 7.2 For estimating the corrosion rate, the sample was connected to the working electrode and a reference electrode was connected by capillary tube in order to make contact with the circuit. A Pt-Ti wire mesh was used as an auxiliary electrode. To ensure that all

other parts were insulated, the sample was painted with electrically nonconductive paint except at the point of interaction. The clamps and plate, which hold the sample, were made of non-conducting polymer. Potential control for corrosion studies was carried out using a Gill AC electrochemical interface (ACM instruments, UK).

In this apparatus, the solution was exposed to air at room temperature, 25^{o}C. It is important to appreciate that in an electrochemical experiment, the measured current is a net quantity being the difference between the anodic and cathodic currents. For polarization experiments carried out in aerated conditions, a background cathodic current due to oxygen reduction will always be present at potentials less than equilibrium potential for this reaction which lies between -0.96 and 0.54 V (SCE). However, where the anodic currents are comparable to the background cathodic current, then the measured anodic current is too small by a constant quantity (i.e. the oxygen reduction current). It is for this reason that many electrochemical tests are carried out under de-aerated conditions. Where deaeration is not practicable, then compensation for the presence of the oxygen reduction current is carried out to extract the correct anodic currents. It should be noted, that in this case, the uncorrected data are reported for the polarization and weight change data in order to reduce errors in the construction of the micro-abrasion-corrosion map.

The sample was prepared by initially grinding the surface to 4000 um and covering the surface with an insulating paint to prevent corrosion current measurements which could be attributed to the unabraded surface.

Micro-abrasion-corrosion tests were carried out at various applied loads (0.5 – 5N) at a constant sliding distance of 3000 rev (235.50 m). The corrosion rates (Kc) during

micro-abrasion corrosion were obtained from the current densities at potentials of -0.4, -0.2, 0, +0.2 V (SCE). The total mass losses due to micro-abrasion wear and corrosion (Kac) at the above potentials were measured after 30 minutes. All the mass loss values reported relate to the metallic component and negligible corrosion of the polymer counterface is assumed for this study.

Composition of Ringer's solution	
Components	**gL^{-1}**
NaCl	8.6
$CaCl_2$	0.33
KCl	0.30

Table 2. Composition of Ringer's solution

Sample material	Co-Cr alloy (Co 61.75, Cr-27, Ni-2.5, Mo 5, C-0.25, Fe-2.5, Si-1) (Weartech Int., USA)
Ball material	UHMWPE (K-mac Plastics, Michigan USA)
Speed	100 rpm
Load	0.5-5 N
Sliding distance	117.78, 29.44, 58.88, 117.75,235.50m (150, 375, 750, 1500, 3000 rev)
Conditions	Corrosive slurry
Slurry	Ringers solution mixed with SiC particles (concentration of

	0.025gcm^{-3})

Table 3. Micro-abrasion-corrosion experimental details

3.1 Materials

The Co-Cr alloy was supplied from Wearech International, CA, USA Table 3. The density was 8386 kgm^{-3} and hardness 386 HV. The UHMWPE ball diameter was 2.2 cm. It was manufactured using injection moulding, and was supplied by K-Mac Plastics.

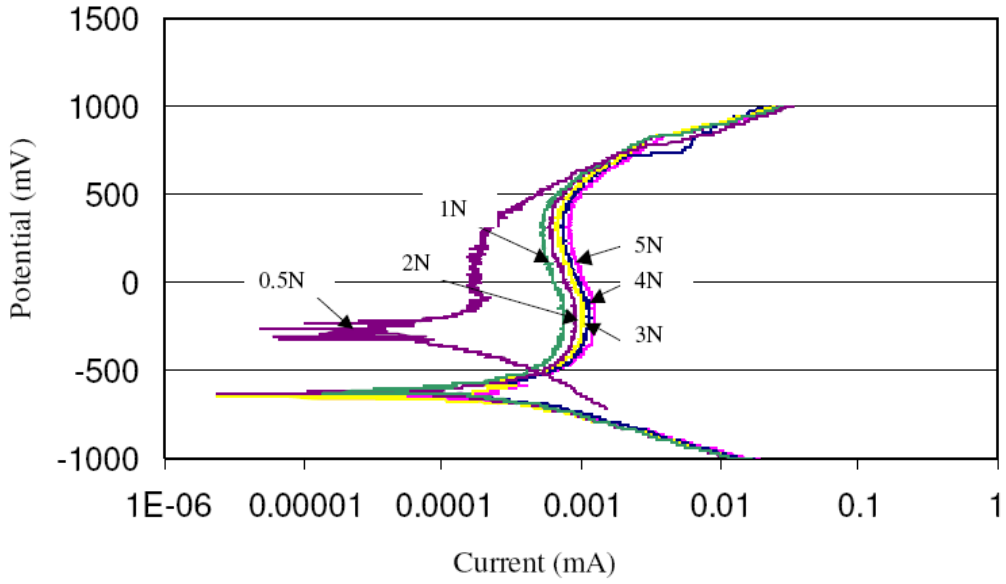

Figure 2(a). In the absence of particles

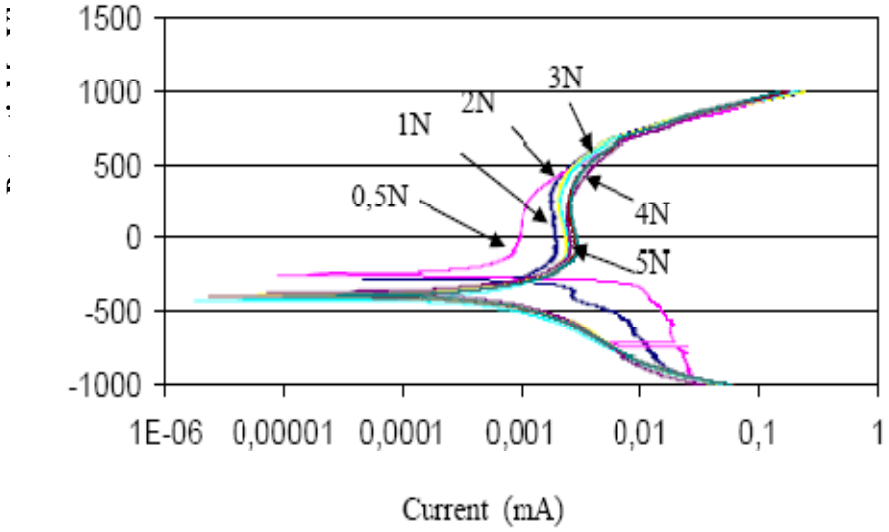

Figure 2 (b). In the presence of particles

Figure 2. Polarization curves in Ringer's solution.

4. Results

4.1 Polarization curves

The polarization behaviour indicated in the absence of particles, Fig. 2(a), for 0.5 N loads it can be seen that the value of Ecorr was higher than for the other loads. In addition, that for Icorr was also slightly lower for 0.5N than the other loads tested. Clear evidence of passivation was indicated at potentials between -0.250 mV and + 250 mV. At this point, a transition to the transpassive regime was accompanied by an increase in current and hence an increase in surface corrosion. This is likely to be due to transpassive oxidation of the chromium ions from Cr^{+3} to Cr^{+6} and has been observed elsewhere (6).

The remaining polarisation curves (1-5N) demonstrated similar behaviour with near identical values of Ecorr and Icorr. It should be noted, however, that for higher values of load, the polariation curves were observed to follow the more traditional S- shaped curve. At 0.5N, the passive regime was identified by a near steady current with increases in anodic potential, whereas for higher loads the current was observed to decrease slightly with increases in anodic potential before finally moving into the transpassive regime. There appears to be a critical load between 0.5 and 1N, where the corrosion current increases significantly.

With increasing load, Fig. 2(b), the anodic current shifted to higher values in the presence of particles. It should be noted that the value of Ecorr was marginally higher for loads 1-5N in the presence of SiC particles than their absence. The current values were higher than those in the absence of particles although there was little difference between these values at higher loads.

.3 Weight change results

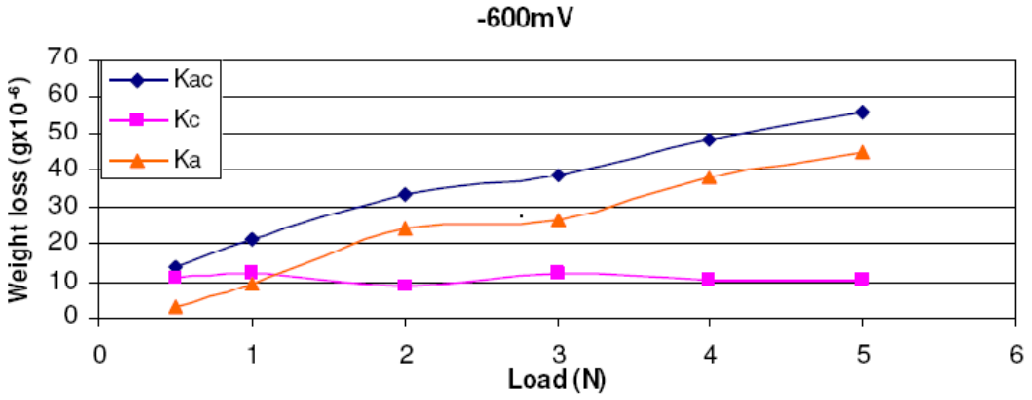

Fig. 3(a) -600 mV

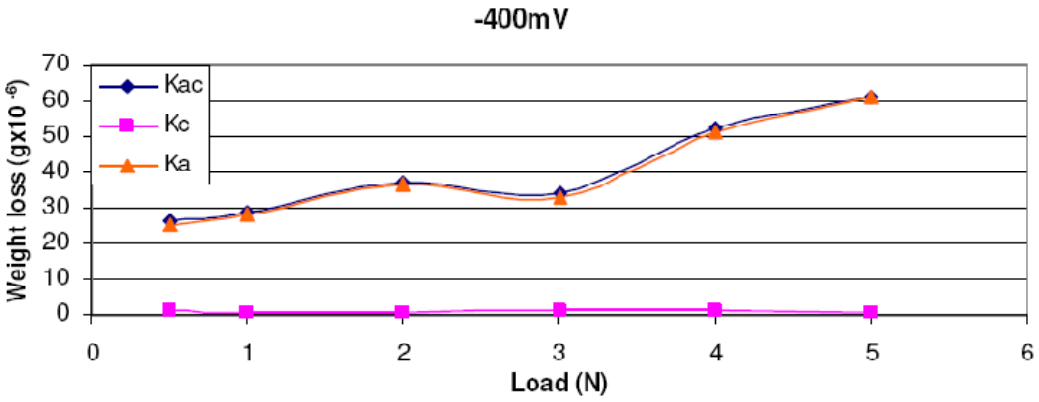

Fig.3(b) -400 mV

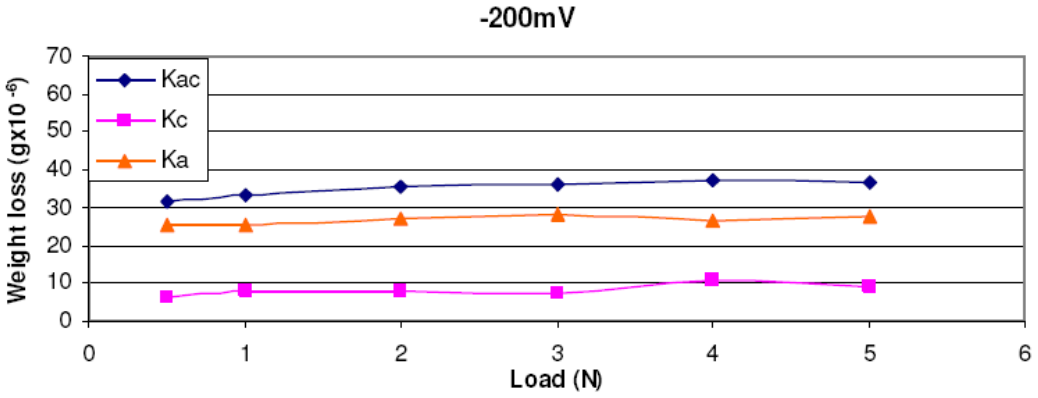

Fig. 3(c) -200 mV

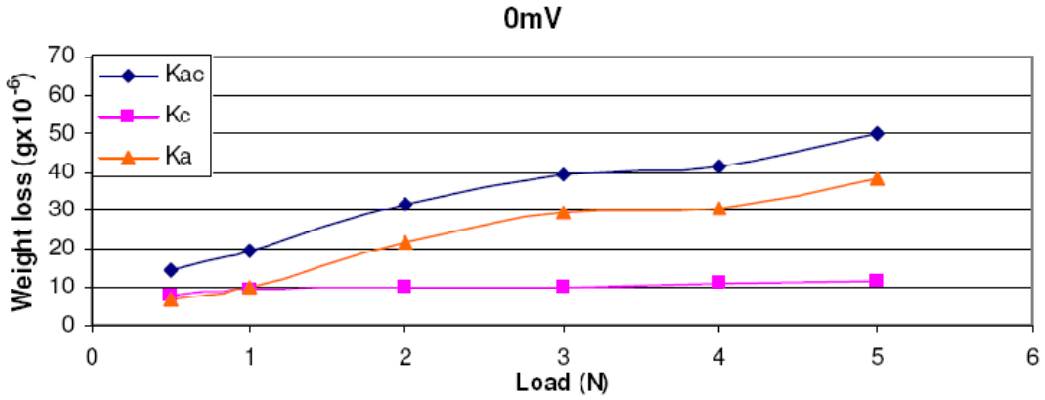

Fig. 3(d) 0 mV

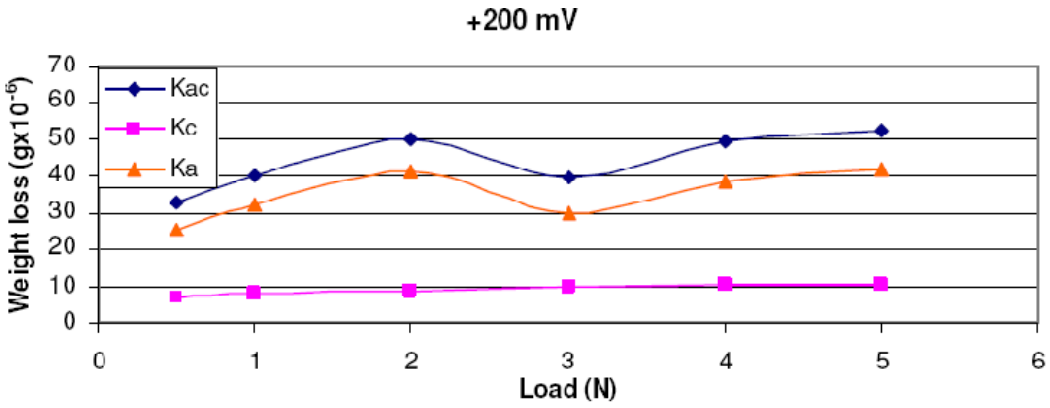

Fig. 3(e) +200 mV

Fig. 4. Weight change data at a range of applied potentials

The weight change data may be explained by defining the following terms, using the wear-corrosion analysis developed by Yue and Shi (16):

If: $K_{ac} = K_a + K_c$ (2)

where, Kac is the total micro-abrasion-corrosion, Ka is the total micro-abrasion rate, and Kc is the total corrosion rate.

Ka can be written as $K_{ao} + \Delta K_a$, i.e.:

$K_a = K_{ao} + \Delta K_a$ (3)

where Kao is the micro-abrasion rate in the absence of corrosion, Δ Ka is the effect of corrosion on the micro-abrasion.

Kc can be written as $K_{co} + \Delta K_c$, i.e:

$K_c = K_{co} + \Delta K_c$ (4)

where Kco is the corrosion rate in the absence of wear, ΔKc is the effect of micro-abrasion on the corrosion, or the enhancement of corrosion due to the micro-abrasion process.

Hence, the total micro-abrasion – corrosion rate can be given as follows:

$K_{ac} = K_{ao} + \Delta K_a + K_{co} + \Delta K_c$ (5)

The results of the various contributions to weight change are given in Table 4. The corrosion rate data, Kc, were derived using Faraday's law, e.g.

$$Kc=Q(ZF)^{-1} \quad (6)$$

$$Kc=Mit(ZF)^{-1} \quad (7)$$

where Q is the charge passed, F is Faraday's constant (96500 C), Z is the number of electrons involved in corrosion process, I, the total current, t the exposure time and M is the atomic mass of the material.

The weight loss due to wear in the absence of corrosion, Kao, was estimated by measuring the weight change in cathodic conditions i.e. at –0.96 V.

The weight change results at, Fig. 3 (a) indicated an increase in mass loss, Kac, with increasing applied load at -600 mV. A generally similar increase in the value of Kac with increasing load was observed at -400mV, Fig. 3(b) . Here, the fact that there was little difference between the values of Kac and Ka demonstrated that corrosion had a negligible role in the overall mass loss rate. For further increases in applied potential at -200 mV, Fig. 3(c) indicated values of Kac, Kc and Ka were largely independent of applied load. However, at more positive applied potential, Fig. 3(d), 0 mV, the overall values of Kac and Ka again increased with applied load. At this potential, at 0.5 N, the value of Kc was marginally greater than Ka, a trend which reversed at

higher potentials, indicating a change in abrasion-corrosion regime as a function of applied load.

At the highest potential value studied, Fig. 3(e), +200 mV, there was a decrease in the values of Kac and Ka at 3 N which reversed at higher loads. The possible reasons for this are discussed below. However, the reproducibility of the results was also evaluated, Fig. 5, and indicates that small deviations may be within the error in the experiment. The reproducibility was estimated to be within ±20%.

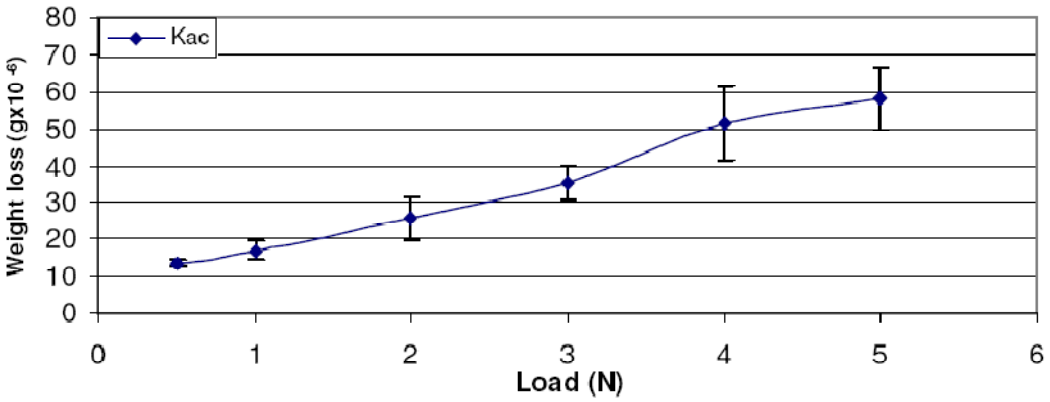

Fig.4 Variation in weight loss, Kac, at 0V, with increasing applied load showing the experimental error in the data based on two consecutive readings at each load.

5. Discussion

5.1 Analysis of weight change and polarization behaviour

The general increasing trend of weight loss (Fig.3 (a-e)) with increasing load is consistent with the Archard theory of wear where the wear rate continually increases with increasing load (16). It is interesting that the corrosion rate Kc, which includes two terms, the corrosion in the presence and the absence of abrasion, Kco + ΔKc, is largely independent of load, which indicates the above a critical load at a given potential, the abrasive action of the particles cannot remove any further passive film on the surface as identified by the polarization data. This pattern is also indicative of a micro-abrasion enhanced corrosion phenomenon.

The results also indicate that the interactions between corrosion and micro-abrasion are enhanced at low loads. However, this is not the case at all anodic potentials. For example, at 0 mV, the value of Kc is marginally greater than Ka at 0.5 mV and approximately equal to Ka at 1 N. At higher loads the situation revereses and the value of Ka exceeds that of Kc. This identifies a change in micro-abrasion-corrosion mechanism, from passivation affected to micro-abrasion affected behaviour at such potentials. Surprisingly, such trends are not observed at more positive potentials and this may be attributed to the decrease in corrosion currents at more anodic values as observed in the polarization data, Fig. 2.

The reduction in micro-abrasion rate at intermediate loads i.e. at 3 N at 0 mV, Fig. , 3(e), has also been observed for pure metals (17). This has been attributed to a transition to a 2 body ridging mechanism where above a critical load, the micron sized particles may entrain in grooves in the surface and the surfaces may become into contact resulting in heat generation and/or associated processes such as thermal softening and oxidation. It also may be due to the error in the experiment, as indicated in Fig. 4. Below a critical particle size, a transition from a micro-abrasion dominated process to a sliding action is anticipated once the particles are small enough to remain in the grooves formed by the gouging action of the particles. Various transitions in micro-abrasion have been the subject of extensive study (6, 17-18). However, it is not possible at this stage to state whether such behaviour observed above can be attributed to such a process.

It is acknowledged that the highest load tested, 5N, represents a force which is artificially high for potential application to bio-implants. For the TE 66 apparatus, it also represents a high value for this test. However, the purpose of this study was to investigate using an accelerated test methodology the various possible regimes for a bio-material couple and hence the wide range of load values used in the study.

5.3 Micro-abrasion-corrosion maps

. 5

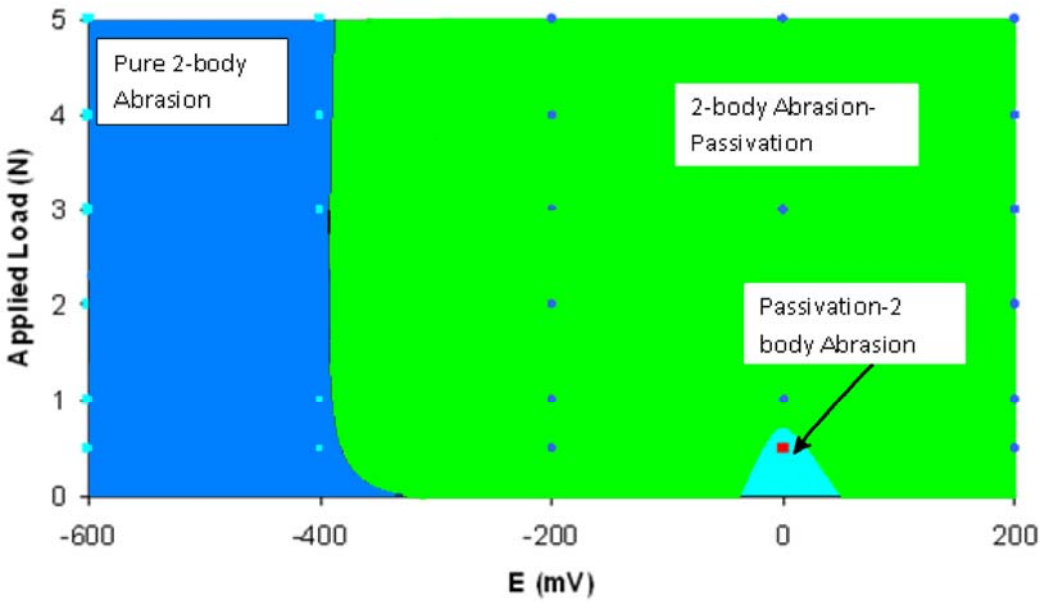

Fig. 5 (a) Mechanism map

The results, Tables 4 and 5, were used to construct micro-abrasion-corrosion maps. The mechanism map is based on the criteria

$$Kc/Ka < 0.1 \quad \text{Micro-abrasion} \qquad (8)$$

$$1> \quad Kc/Ka \geq 0.1 \quad \text{Micro-abrasion-corrosion} \qquad (9)$$

$$1 \geq \quad Kc/Ka > 1 \quad \text{Corrosion-micro-abrasion} \qquad (10)$$

$$Kc/Ka > 10 \quad \text{Corrosion} \qquad (11)$$

The micro-abrasion process was identified as 2-body based on the Adachi and Hutchings analysis (19) for the conditions studied.

It is clear, from the results, Fig. 5(a) that at cathodic potentials less than -400 mV, micro-abrasion is dominant. Above such values, the wastage mechanism changes to 2 body abrasion-passivation apart from in the region of 0 mV, where a transition to passivation-2 body abrasion takes places. This indicates the combination of conditions where corrosion is more dominant than abrasion.

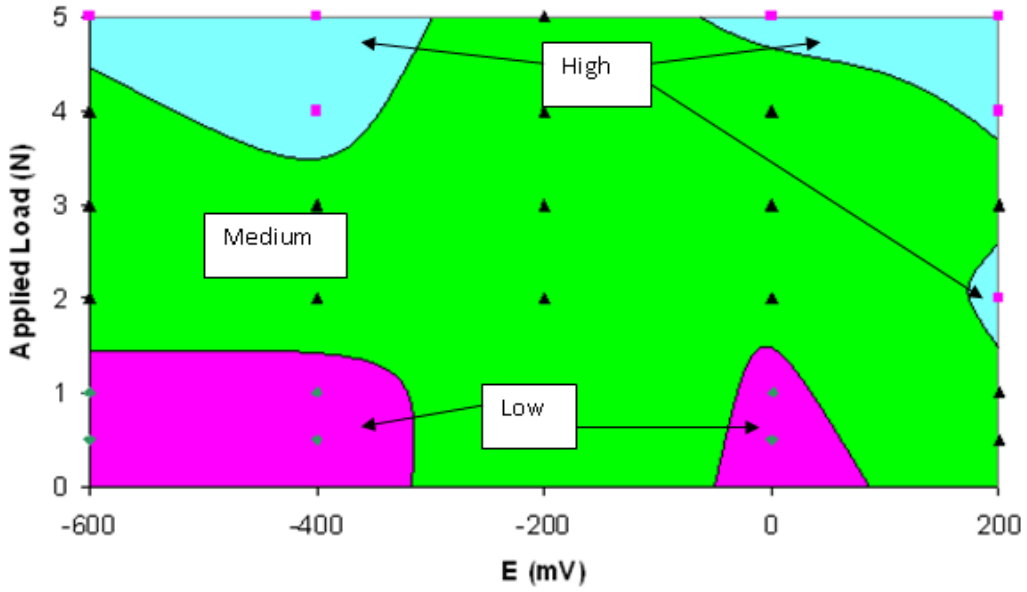

Fig. 5 (b) Wastage Map

In the construction of a wastage map for the results, Fig. 5(b), the following criteria are used to set the limits.

	$Kac \leq 3 . 10^{-6} g$	Low	(12)
$3 . 10^{-6} g <$	$Kac \leq 6 . 10^{-6} g$	Medium	(13)
	$Kac > 6 . 10^{-6} g$	High	(14)

The results indicate that when the alloy passivates in Ringer's solution, the process has the effect of marginally reducing the wastage rate except at high potentials. The beneficial effect of formation of the chromium oxide passive film is particularly evident in the region centred around 0 mV and between 1 and 2N. This suggests that there may be an optimum electrochemical equilibria /tribological condition where wear may be minimized in body fluids of comparable concentration. If tribo-corrosion occurs as a result of smaller particles in hip joint contacts i.e.by nano paricles as has been suggested in recent work, it may be interesting to see how such maps would appear for the effects of these particles. (20)

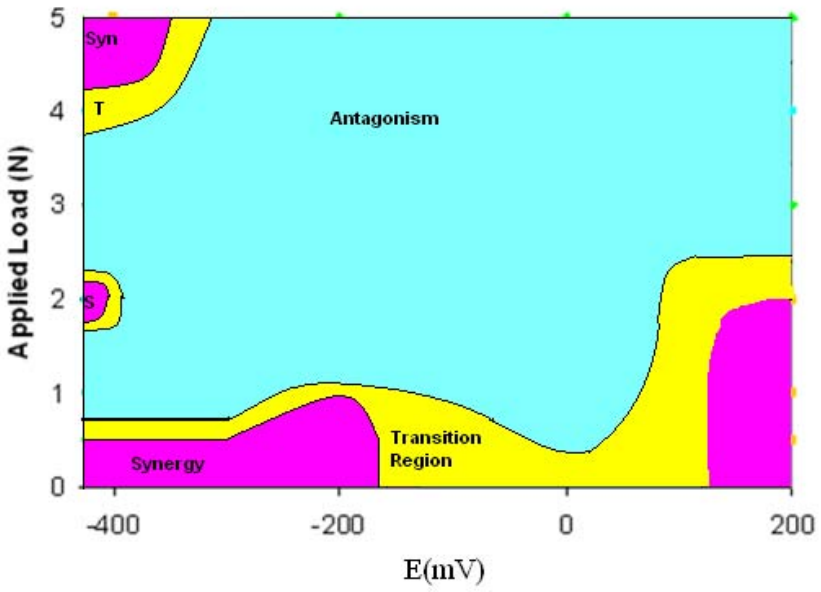

Fig. 5 (c) Synergy map

Fig. 5. Micro-abrasion-corrosion maps for Co-Cr/UHMWPE in Ringer's solution

In order to investigate the trends in the results further, Tables 4-5, micro-abrasion-corrosion synergy maps were constructed using the following limits as defined in other work (21-24).

$\Delta Ka/\Delta Kc \leq 0.1$	Additive	(15)
$1 \geq \Delta Ka/\Delta Kc > 0.1$	Additive-Synergistic	(16)
$\Delta Ka/\Delta Kc > 1$	Synergistic	(17)

If the inequalities are negative, then "synergistic" is replaced by "antagonistic" behaviour. The results, Fig. 5 (c) indicate that the map is largely dominated by antagonistic behaviour.

Using the error estimation of ±19.5 % which was obtained from Fig. 4, all values of ΔKa and ΔKc were modified in the positive and negative directions to their extreme error values. The resulting synergy/antagonism levels were then recalculated for each error modified scenario to investigate whether the original defined regime would still remain at the extreme values or possibly transition into a new regime.

(It should be noted that most of the original values of $\Delta Ka/\Delta Kc$ remained unaltered. However, various isolated regions in the map are now included in a transition region outlined in the diagram which includes the additive - antagonistic or additive- synergy regimes. The authors have decided that grouping these values together is acceptable

as these values are relatively small in comparison with some of the larger synergy and antagonism values.)

At low loads, i.e. less than 1.5 N, the synergistic effect changes to antagonistic in the region of 0 mV. This reverts to synergistic behaviour at higher potentials. This indicates that the corrosion conditions under which this passive film of chromium oxide forms are the optimum for the exposure conditions, in which an applied stress is imposed. Hence, they indicate that the film is generally providing protection under this window of conditions. The transition to transpassive behaviour at higher potentials as observed from the polarization data results in micro-abrasion-corrosion process where the film is commencing to break down.

The results are interesting in that they demonstrate that for application to bio-medical conditions i.e. a hip/joint for patient A of relatively high activity i.e. a professional sports person, if a potential range could be identified for the tribo-corrosion behaviour for such an individual, then some projection of lifetime could be made based on the mapping methodologies above. This could lead to a decision to replace the joint with a metallic material or with the same material with a surface coating. However, further research is necessary to realize the practical applications of such work to real life conditions.

Hence, it is shown that by using tribo-corrosion mapping methodologies above, optimum electrochemical and tribological parameters may be identified for bio-implant materials using the micro-abrasion test apparatus. The application of such results to in-vivo conditions will involve knowledge of the electrochemical and

tribological variables together. Further work will be to investigate how such diagrams can be applied to other hip joint material couples, including addressing mathematical models of tribo-corrosion mapping development as in recent work (24), in addition to other biological conditions involving implants.

6. Conclusions

(i) The micro-abrasion-corrosion behaviour of a Co-Cr/UHMWPE couple has been investigated in Ringer's solution, by investigating the effect of applied load over a range of potentials in potentiostatic and potentiodynamic conditions.

(ii) The results have indicated various trends on the effect of load as a function of increasing potential, with corrosion dominating the abrasion at low loads, at anodic potentials, where passive film formation is favoured.

(iii) Micro-abrasion-corrosion maps have been constructed using such an approach demonstrating variation in mechanisms, wastage and synergism//antagonism in the tribo-corrosion processes.

(iv) Over the potential range studied, strong evidence of antagonism has been observed, indicating that the chromium oxide layer formed on the surface was resistant to the micro-abrasion conditions. The ability of this film to

provide protection has been found to be dependent on the load and potential.

Acknowledgements.

MMS writes. This paper is dedicated to two family members, my father of 92, Maurice Stack, whose issues in relation to his locomotion in his advancing years have inspired my interest in this area, and my sister Maria, a GP , who with a diploma in Geriatric Medicine, is eminently more qualified than me in these areas.

References

1. J. J. Callaghan, A.G. Rosenberg, H.E Rubash, Lippincott, *The adult hip*, Williams and Wilkins, 2nd Ed, Philadelphia, USA, 2007.
2. J. J. Jacobs, J.L. Gilbert and R.M. Urban,"Corrosion of metal orthopaedic implants". *J Bone Joint Surg Am* 80, 268–*282.*
3. H. Yoshida, A. Faust, J. Wilckens, M. Kitagawa, J.Fetto and E. Chao, (2006) "Three-dimensional dynamic hip contact area and pressure distribution during activities of daily living', *Journal of Biomechanics*, Vol. 39, 1996–2004.
4. R . Büscher and A. Fischer, "Metallurgical Aspects of Sliding Wear of FCC Materials for Medical Applications", (2003). *Materialwissenscgaft und Werkstofftechnik*, 34, 966.
5. M.A. Wimmer, C. Sprecher, R. Hauert, G Täger and A. Fischer, (2003), "Tribochemical Reaction on Metal-On-Metal Hip Joint Bearings - A Comparison between in-vitro and in-vivo results". *Wear*, 255, 1007
6 D. Sun, J.A. Whharton, R.J.K. Wood, and W.M. Rainforth, (2009), "Microabrasion-corrosion of cast CoCrMo alloy in simulated body fluids". *Tribology International*, 42, (1), 99-110.
7. M. M. Stack , H. Jawan and M.T. Mathew, (2005), "On the construction of micro-abrasion maps for a Steel/Polymer couple in corrosive environments", *Tribology International*, 38 (9), 848-856.
8. M.R. Thakare, J.A. Wharton., R.J.K. Wood and C. Menger, (2007), "Exposure effects of strong alkaline conditions on the microscale abrasion-corrosion of D-gun sprayed WC-10Co-4Cr coating", *Tribology International*, 41 (7), 629-639.

9. M.R. Thakare, J.A. Wharton, R.J.K. Wood and C. Menger, (2007), "Exposure effects of alkaline drilling fluid on the microscale abrasion-corrosion of WC-based hardmetals", *Wear*, 263 (1-6), 125-136.
10. I.M. Hutchings and K.L. Rutherford, (1997),"Theory and Application of a Micro-Scale Abrasive Wear Test". *J Test Eval*, *JTEVA*, 25(2), 250-260.
11. J. Ingram, J.B. Matthews J. Pipper, M. Stone and J Fisher, (2002),"Comparison of the biological activity of grade GUR 1120 and GUR 415HP UHMWPE wear debris", *Bio-Med Mater Eng*, 12(2), 177-188.
12. ASTM, F75: Standard specification for cast cobalt-chromium-molybdenum alloy for surgical imlant applications, in :Annual Book of ASTM Standards: Medical Devices and Services, (1998) 13.01, American Society for Testing and Materials, Philadelphia, PA, 10.4-6
13. Y. S. Li., K Wang., P He., B. X. Huang., P. Kovacs, (1999),"Surface enhanced Raman spectroelectrochemical studies of corrosion films on implant Co-Cr-Mo alloy in biosimulating solutions", *J Raman Spectrosc*. 30 (2), 97-103.
14. A. W. Hodgson., S Kurz., S. Virtanen, V. Fervel, C.O.A Olsson and S. Mischler, (2004),"Passive and transpassive behaviour of CoCrMo in simulated biological solutions", *Electrochim. Acta*, 49 (13), 2167-2178.
15. Z. Yue, P. Zhou, J. Shi, In: K. C. Luedema, editor.(1987) *Proceedings of conference on wear of materials*. New York:ASME:.763-768.
16. J.F. Archard., (1953),"Contact and rubbing of flat surfaces", *J.Appl.Phys.*, 24 (8), 981.
17. M.M Stack M. M., Mathew., (2003),"Micro-abrasion transitions of metallic materials", *Wear*, 255 (1-6), 14-22.

18. R.I Trezona and I.M. Hutchings, (1999),"Three-body abrasive wear testing of soft materials", *Wear*, 233, 209-221.
19. K. Adachi and I.M Hutchings, (2003)," Wear-mode mapping for the micro-scale abrasion test", *Wear*, 255, 23-29.
20. Y. Yan, A. Neville, D. Dowson, S. Williams, J. Fisher, (2009), Effect of metallic nanoparticles on the biotribocorrosion behaviour of Metal-on-Metal hip prostheses, *Wear*, 267, 5-8, 683-688.
21. M.M. Stack and T.M Abd El Badia (2006),"On the construction of erosion-corrosion maps for WC/Co-Cr- based coatings in aqueous conditions", *Wear*, 261 (11-12), 1181-1190.
22. M.M. Stack and T.M. Abd El Badia, (2008) "Some comments on mapping the combined effects of slurry concentration, impact velocity and electrochemical potential on the erosion-corrosion of WC/Co-Cr, *Wear*, 264, 826-837.
23. M.M. Stack and G.H. Abdulrahman, (2010)"Mapping erosion-corrosion of carbon steel in oil exploration conditions: Some new approaches to characterizing mechanisms and synergies", *Tribology International,* Available on-line 20 January 2010, doi:10.1016/j.triboint.2010.01.005
24. M.M. Stack, S.M. Abdelrahman and B.D. Jana (2010), "A new methodology for modelling erosion-corrosion regimes of real surfaces: gliding down the galvanic series for a range of metal corrosion systems", *Wear,* 268, 3-4, 533-542, 2010.

Table 4: Kc/Ka values at various potentials

Potential mV/SCE	Kac (g x10^{-6})	Kc (g x10^{-6})	Ka (g x10^{-6})	Kc/Ka
(a) 0.5N Applied Load				
-600	14.05	10.96	3.084	3.55
-400	26.41	1.05	25.36	0.04
-200	31.41	6.14	25.27	0.24
0	14.34	7.55	6.79	1.11
200	32.48	6.97	25.51	0.27
(b) 1N Applied Load				
-600	21.23	12.02	9.22	1.30
-400	28.83	0.37	28.45	0.01
-200	33.03	7.83	25.21	0.31
0	19.32	9.25	10.07	0.92
200	40.18	8.04	32.14	0.25
(c) 2N Applied Load				
-600	33.03	8.73	24.30	0.36
-400	37.08	0.63	36.45	0.02
-200	35.30	8.08	27.23	0.30
0	31.41	9.75	21.66	0.45
200	49.93	8.49	41.44	0.20
(d) 3N Applied Load				
-600	38.30	11.84	26.46	0.45

-400	34.15	1.12	33.03	0.03
-200	35.89	7.38	28.50	0.26
0	39.55	10.01	29.53	0.34
200	39.55	9.73	29.82	0.33
(e) 4N Applied Load				
-600	48.44	10.48	37.96	0.28
-400	52.23	1.05	51.18	0.02
-200	37.08	10.48	26.60	0.39
0	41.48	10.96	30.53	0.36
200	49.18	10.48	38.70	0.27
(f) 5N Applied Load				
-600	55.42	10.41	45.00	0.23
-400	61.34	0.40	60.95	0.01
-200	36.48	8.89	27.59	0.32
0	49.93	11.50	38.43	0.3
200	52.23	10.25	41.98	0.24

Table 5: ΔKa/ΔKc values at various potentials

Potential mV/SCE	ΔKa ($g \times 10^{-6}$)	ΔKc ($g \times 10^{-6}$)	ΔKa/ΔKc	Effect
(a) 0.5N Applied Load				
-400	11.02	0.88	12.57	Synergy
-200	10.93	6.06	1.80	Synergy
0	-7.55	7.38	-1.02	Antagonistic
200	11.17	6.77	1.65	Synergy
(b) 1N Applied Load				
-400	11.60	-0.07	-158.40	Antagonism
-200	8.35	7.35	1.14	Synergy
0	-6.79	8.80	-0.77	Additive-Antagonistic
200	15.28	7.62	2.00	Synergy
(c) 2N Applied Load				
-400	4.51	0.13	34.05	Synergy
-200	-4.72	7.54	-0.63	Additive-Antagonistic
0	-10.28	9.26	-1.11	Antagonism
200	9.49	8.05	1.18	Synergy
(d) 3N Applied Load				
-400	-27.44	0.60	-45.42	Antagonism
-200	-31.97	6.76	-4.73	Antagonism
0	-30.94	9.50	-3.26	Antagonism
200	-30.65	9.26	-3.31	Antagonism

(e) 4N Applied Load

-400	5.62	0.51	11.00	Synergy
-200	-18.96	9.52	-1.99	Antagonism
0	-15.03	10.42	-1.44	Antagonism
200	-6.86	9.99	-0.69	Additive-Antagonistic

(f) 5N Applied Load

-400	-0.40	-0.34	1.18	Synergy
-200	-33.75	7.82	-4.31	Antagonism
0	-22.91	10.74	-2.13	Antagonism
200	-19.37	9.73	-1.99	Antagonism

Captions for tables

1. Specification of micro-abrasion apparatus

2. Composition of Ringer's solution

3. Micro-abrasion-corrosion experimental details

4. Kc/Ka values at various potentials

5. ΔKa/ΔKc values at various potentials

Captions for Figures

1. Micro-abrasion corrosion apparatus

2. Polarisation curves at various loads in Ringer's solution

   (a) In the absence of particles

   (b) In the presence of particles

3. Variation of weight change during the micro-abrasion-corrosion process

   (a) – 0.600 mV

   (b) –0.400 mV

   (c) –0.200 m V

   (d) 0 mV

   (e) +0.200 mV

4. Variation in weight loss, Kac at 0.2 V, with increasing applied load showing the experimental error in the data based on two consecutive readings at each load.

5. Micro-abrasion corrosion maps for the Co-Cr/UHMWPE couple in Ringer's solution.

   (a) Mechanism map

(b) Wastage map

(c) Synergy map